RSC Advances

PAPER

View Article Online
View Journal | View Issue

Cite this: *RSC Adv.*, 2014, **4**, 14971

The particle proximity effect: from model to high surface area fuel cell catalysts†

Jozsef Speder,*[a] Lena Altmann,[b] Marcus Bäumer,[b] Jacob J. K. Kirkensgaard,[c] Kell Mortensen[c] and Matthias Arenz*[a]

Received 10th January 2014
Accepted 13th March 2014

DOI: 10.1039/c4ra00261j

www.rsc.org/advances

In this work, Pt nanoparticles prepared by a colloidal method are supported on high surface area carbons. The electrocatalysts synthesized by this method have well-separated, size-controlled nanoparticles with tunable interparticle distance, and thus enable the examination of the particle proximity effect on the oxygen reduction reaction (ORR). The particle proximity effect proposes that the activity of fuel cell catalysts depends on the distance between the catalyst particles and is here for the first time demonstrated for high surface area catalysts; *i.e.* catalysts which can be used in fuel cells. Based on rotating disk electrode (RDE) experiments, we show that the kinetic current density of ORR depends on the distance between the neighboring nanoparticles, *i.e.* the ORR activity increases with decreasing interparticle distance.

1. Introduction

Proton exchange membrane fuel cells (PEMFCs) powered by hydrogen or methanol, are promising clean energy converting devices with high efficiency. Such energy converters can be used in a wide range of mobile and stationary applications.[1–3] The current electrocatalyst of choice for PEMFCs is based on platinum (Pt) or Pt alloy nanoparticles (NPs) dispersed on a high surface area (HSA) carbon support.[4] However, the high cost of Pt raises a significant challenge for the commercial viability of PEMFCs. In order to improve the platinum utilization extensive research is devoted to gain a better understanding of the structure–activity relationship of PEMFC catalysts for the oxygen reduction reaction (ORR).

The effect of the Pt particle size on the ORR activity using "bare" Pt NPs or dispersed on a HSA carbon support has been the subject of several investigations by different researchers and is controversially debated in literature.[1,4–7] Some studies claim that not only the particle size but the maintenance of a sufficient interparticle distance plays a crucial role in achieving and maintaining high ORR activity.[8–13] According to this theory only if Pt particles are highly dispersed (well-separated from neighboring particles) on the support, the full electrochemical surface area (ECSA) is utilized and O_2 molecules are supplied by spherical diffusion to the individual particles. Only under such conditions a high surface specific activity (I_s) and mass specific activity (I_m) can be achieved. In contrast, if Pt particles are close together, the "territories" (diffusion fields) of the catalyst particles for O_2 overlap, resulting in decreased activities for the ORR. In all these studies, however the experimental investigation of this phenomenon concerning highly dispersed Pt NPs was limited by the fact that they were carried out on relatively poorly defined catalysts prepared by traditional synthesis routes (impregnation, precipitation) where an increase in the metal weight loading (decreasing interparticle distance, ipd) results in an increase of the Pt NP size. To overcome this problem and to investigate the effect of the particle proximity on the ORR activity, our previous work was conducted on well defined, size selected Pt nanoclusters.[14–16] Our recent study revealed that the electrocatalytic ORR activity can be influenced by changing the interparticle distance between neighboring Pt nanoclusters.[16] To utilize this knowledge for the design of industrial PEMFC catalysts and to prove the particle proximity effect on such catalysts, in this study catalyst samples were prepared by the recently introduced Pt/C toolbox synthesis method.[17] In this approach carbon supported, Pt based catalysts are prepared from a colloidal suspension of well-defined Pt NPs synthesized by an ethylene glycol method.[18] The particles are highly monodisperse and typically around 2 nm in diameter. In addition, the particles are free of any strongly binding surfactants or other agents and no heat treatment steps are required. Using this controlled synthesis a varying Pt to carbon ratio leads to a changing interparticle distance between the NPs, *i.e.* the interparticle distance can be uniquely tuned. Therefore, the obtained electrocatalysts are ideally suitable for the examination of the particle proximity effect on the ORR.

[a]*Nano-Science Center, Department of Chemistry, University of Copenhagen, Universitetsparken 5, DK-2100 Copenhagen Ø, Denmark. E-mail: spederj@outlook.com; m.arenz@chem.ku.dk*

[b]*Institute of Applied and Physical Chemistry and Center for Environmental Research and Sustainable Technology, University Bremen, D-28359 Bremen, Germany*

[c]*Niels Bohr Institute, University of Copenhagen, Universitetsparken 5, DK-2100 Copenhagen Ø, Denmark*

† Electronic supplementary information (ESI) available. See DOI: 10.1039/c4ra00261j

To determine the effect of varying interparticle distance on the ORR, the catalyst activity is characterized by rotating disk electrode (RDE) measurements using the thin film approach.[19] In order to ensure a sufficient O_2 diffusion to the Pt catalyst particle surface we applied an ultra-thin and uniform dispersion of Pt catalyst on the glassy carbon (GC) disk.[20–22] In the present work we show that the kinetic current density of the ORR strongly depends on the distance between the neighboring NPs, *i.e.* that the particle proximity effect also exists for industrial, carbon supported PEM fuel cell catalysts.

2. Experimental section

2.1 Catalyst material synthesis

The investigated catalysts, hereafter called Pt/C, were synthesized in-house according to ref. 17. The synthesis of the electrocatalysts consists of two main steps. First, a suspension of colloidal Pt NPs with narrow size distribution is prepared *via* an ethylene glycol (EG) route. A detailed description of the Pt NP preparation method can be found in ref. 18. Briefly, a colloidal suspension of Pt NPs is synthesized by mixing an ethylene glycol solution of NaOH (50 mL, 0.5 M) with an ethylene glycol solution of $H_2PtCl_6 \cdot xH_2O$ (50 mL, 1.0 g) under vigorous stirring resulting in a yellowish platinum hydroxide or oxide colloidal solution. The reaction is performed under an inert atmosphere of Ar. The colloidal solution is then heated to 160 °C while purging Ar gas through the system for 3 h obtaining a blackish-brown homogeneous metal particle colloidal suspension. The size and structure of the thus synthesized Pt NPs is controlled by transmission electron microscopy (TEM). The average diameter of the obtained Pt NPs is typically around 2 nm exhibiting a narrow size distribution. In the next step the NPs are deposited in varying amounts onto the HSA carbon support, *i.e.* Ketjenblack EC-300J (AkzoNobel, Brunauer–Emmett–Teller (BET) surface area: 795 $m^2\ g^{-1}$) or Vulcan XC72R (Cabot Corporation, BET area: 235 $m^2\ g^{-1}$). In order to support the Pt NPs onto a HSA carbon 40 mL of 1 M HCl was added to the colloidal NP solution for precipitation. The solution was centrifuged (4000 rpm, 6 min) and repeatedly washed in HCl before dispersing it in acetone. Finally, the as-synthesized Pt NPs were deposited onto different HSA carbons by mixing the NPs suspension with carbon black in 3 mL of acetone and sonicating for 1 h. Finally the catalyst was dried.

Pt/C samples were prepared with different nominal Pt loadings between 2 and 90 wt% Pt. The actual Pt content of the catalysts was analyzed by ICP-MS (NexION 300X, Perkin Elmer) through a Meinhard quartz nebulizer and a cyclonic spray chamber, operating at nebulizer gas flow rates of between 1 and 1.02 L min^{-1} (Ar, purity 5.0). Before ICP analysis, the catalysts were dissolved in inverse *aqua regia* (the volume ratio of HCl to HNO_3 was 1 : 3) and then diluted. The nominal and the actual Pt loading values agreed within 10–30%. As a general trend the difference decreased with higher loadings. For the calculation of the electrochemically accessible surface area (ECSA) and the mass activities the actual Pt loading values were used.

2.2 Electrochemical characterization

The electrochemical measurements were performed using a computer controlled, home-built potentiostat and a rotating disk electrode (RDE) setup. The electrochemical cell was a home-built Teflon cell based on a three-compartment configuration. The counter (auxiliary) electrode was a platinum mesh, the reference electrode a Schott Ag/AgCl/KCl(sat) electrode placed in a separated compartment separated by an additional Nafion® membrane in order to avoid the diffusion of Cl^- ions into the main compartment.[23] All potentials in this work are referred to the reversible hydrogen electrode (RHE) potential, which was experimentally determined for each measurement series. All electrolyte solutions were prepared with Millipore® water (>18.3 MΩ cm, TOC < 5 ppb). $HClO_4$ and HCl were from Merck (suprapur). The measurements were performed at 20 °C. Prior to the RDE measurements the glassy carbon (GC) working electrode (5 mm diameter, 0.196 cm^2 geometrical surface area) was polished to mirror finish using alumina oxide paste 0.3 and 0.05 μm (Buelher-Met, deagglomerated α-alumina and γ-alumina, respectively), and cleaned ultrasonically in ultrapure water and cc. 70 wt% $HClO_4$. The catalyst ink was prepared by ultrasonically dispersing the catalyst powder in ultrapure water (0.14 $mg_{Pt}\ cm^{-3}$). A volume of 20 μL of the suspension was then pipetted onto the GC electrode leading to a Pt loading of 14 $\mu g_{Pt}\ cm^{-2}$ and thereafter dried in a nitrogen gas stream. Only samples with a uniform catalyst film were analyzed. All electrochemical experiments were performed in 0.1 M $HClO_4$ solution. Prior to the measurements the electrolyte was de-aerated by purging with Ar gas (99.998%, Air Liquide), and the measurements were started with cleaning the catalyst by potential cycles between 0.05 and 1.1 V_{RHE} at a scan rate of 50 mV s^{-1}. The specific activity of the ORR was determined from the positive going RDE polarization curves recorded in O_2 saturated 0.1 M $HClO_4$ solution at a scan rate of 50 mV s^{-1} and at a rotation speed of 1600 rpm. In order to exclusively analyze the ORR current, the polarization curves were corrected for the non-faradaic background by subtracting the CVs recorded in Ar-purged electrolyte. Furthermore, the solution resistance between the working electrode and the Luggin capillary was determined using an AC signal (5 kHz, 5 mV) and thereafter compensated for using the potentiostat's analog positive feedback scheme. The resulting effective solution resistance was less than 3 Ω for each experiment. The ECSA of the catalysts was determined from the CO stripping charge[24] recorded at a sweep rate of 50 mV s^{-1}. The mass activity was calculated based on the specific activity and the ECSA. The latter was determined as the average of several measurements using a multi-electrode setup.[25]

2.3 Transmission electron microscopy (TEM)

The electrocatalysts were characterized by TEM using a Tecnai T20 G2 (Philips FEI, Oregon, USA) equipped with a thermionic electron gun operated at 200 kV. The micrographs were acquired using a Gatan2K UltraScan 1000 CCD camera.

2.4 Small angle X-ray scattering (SAXS)

The platinum particle size distribution of the supported catalysts were determined by Small Angle X-ray Scattering (SAXS) using a SAXSLab instrument (JJ-Xray, Denmark) equipped with a Rigaku 100XL+ micro focus sealed X-ray tube and a Dectris 2D 300K Pilatus detector. On this instrument the detector is moveable allowing different structural length scales to be accessed. Here the magnitude of the scattering vector is defined as $q = 4\pi/\lambda \sin(\theta)$ with λ being the X-ray wavelength and θ half of the scattering angle. Samples were sealed between two 5–7 μm thick mica windows and measurements were performed *in vacuo*. The data analysis follows ref. 17 with small modifications. The scattering data are fitted to the following expression:

$$I(q) = C_1 I_{\mathrm{CARBON}}(q) + C_2 + C_3\Pi(q) + C_4\int P_s^2(q, R)D(R)\mathrm{d}R \quad (1)$$

where C_i are constants and the four terms represent the background from the pure carbon support with no platinum loaded, a small constant background, a term accounting for the pore structure and a term representing the platinum particles, respectively. The I_{CARBON}-term, representing the carbon background can be measured directly for the untreated samples, this is, however, more difficult for the treated samples, because of the degradation of the carbon. In those cases we follow ref. 26 and model the pure carbon as a power law q^{-n}, where exponent n comes out from the fit as *ca.* 3.3 in accordance with ref. 26. The pore structure expressed by the $\Pi(q)$-term is given by the Lorentz expression:

$$\Pi(q) = \frac{a^4}{(1 + a^2q^2)^2} \quad (2)$$

with a being a characteristic pore dimension. The final term, the sphere term $P_s^2(q, R)$ representing the platinum particles is described by a lognormal size distribution, $D(R)$, of spherical particles. The form factor amplitude of a sphere with radius R is given by

$$P_s(q, R) = 4\pi R^3 \frac{\sin qR - qR\cos qR}{(qR)^3} \quad (3)$$

and the log-normal size distribution by

$$D(R) = \frac{1}{R\sigma\sqrt{2\pi}}\exp\left(\frac{-[\ln(R/R_0)]^2}{2\sigma^2}\right) \quad (4)$$

where σ is the variance and R_0 the geometric mean of the lognormal distribution. During the fitting procedure, it was found that at the highest loading degrees a hard-sphere structure factor was required to fit the data. Thus, in those cases this factor is multiplied to the last term in eqn (1). The expression for the hard-sphere structure factor can be found in ref. 27. Basically it depends on the sphere radius and the sphere volume fraction, so it is only relevant at the highest loadings (here EC300 90 wt% and Vulcan 80 wt%). From each particle size distribution $D(R)$, we calculated a volume normalized surface area of each catalyst by using the following equation:

$$\frac{A}{V} = \frac{\sum_i D(R_i)4\pi R_i^2}{\sum_i D(R_i)\frac{4\pi}{3}R_i^3} \quad (5)$$

Assuming mass is proportional to volume, the ratios of these areas are directly compared to the ratios of the ECSA. Further, by dividing this ratio with the platinum density of 21.45 g cm^{-3} absolute numbers per unit mass can be obtained for each sample. The presented model fits are computed using home-written MATLAB code.

2.5 Calculation of the interparticle distance

As interparticle distance (ipd) we define the average distance between the edge of a catalyst particle and the edge of its nearest neighboring catalyst particle given by:[16]

$$i_{\mathrm{pd\,(edge\ to\ edge)}} = \sqrt{\frac{A}{N}} - d_{\mathrm{NP}} \quad (6)$$

where A is the BET surface area of support, N is the number of nanoparticles and d_{NP} is the average diameter of the nanoparticles, determined by SAXS. We assume for the calculation of the interparticle distance that all particles exhibit a spherical shape, the particles are monodispersed and homogenously distributed on the carbon support. A sketch of the interparticle distance is seen in Fig. 1. The theoretical interparticle distance is also compared with TEM micrographs.

3. Results and discussion

3.1 Catalyst characterization

We begin with the description of the catalyst samples used in this study. By applying a colloidal synthesis approach,[17] we prepared catalyst samples consisting of Pt NPs supported on Ketjenblack EC-300J and Vulcan XC72R carbons with nominal Pt loading between 2 and 90 wt%. In Fig. 2, the ECSA values of the prepared samples are summarized as a function of the nominal metal loading and calculated interparticle (edge to edge) distance, respectively. It can be seen that in general a higher electrochemical surface area is achieved on the Vulcan than on Ketjenblack support. For Pt loadings smaller or equal to 70 wt% the average ECSA of the catalyst samples is around 85 and 103 m^2 g^{-1} on Ketjenblack and Vulcan, respectively. This indicates a higher degree of dispersion and utilization of Pt

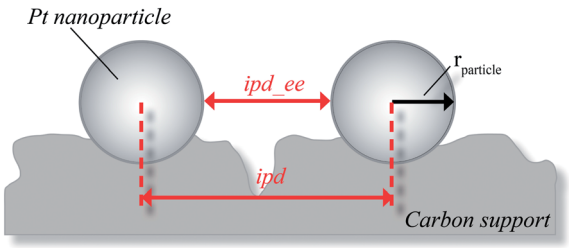

Fig. 1 Model for the calculation of the interparticle distance between two particles.

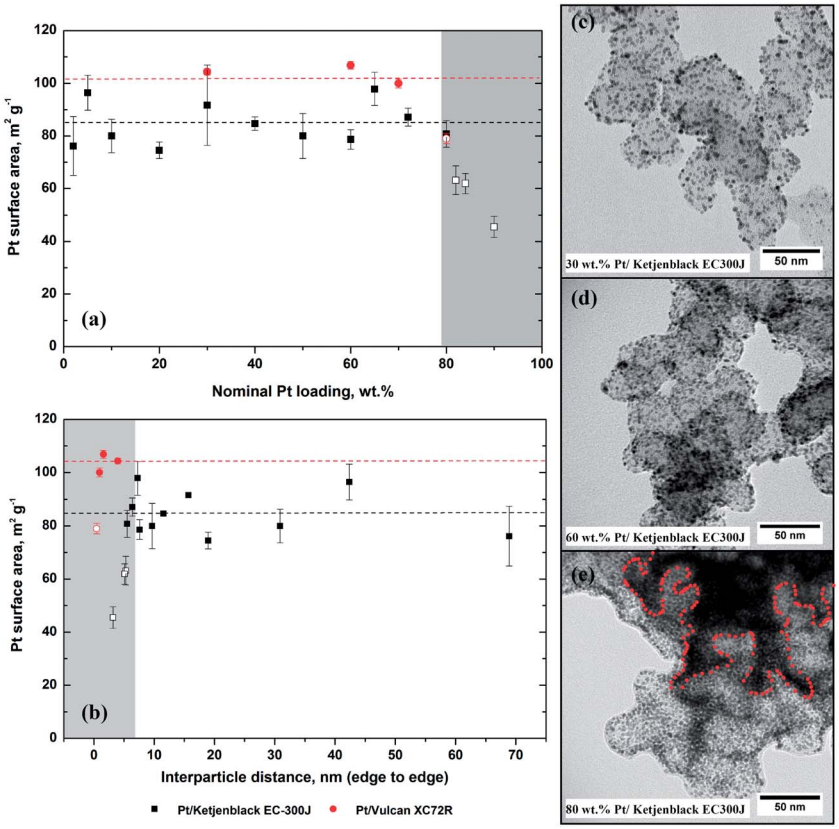

Fig. 2 ECSA of the catalyst samples as a function of the nominal Pt weight loading (a) and calculated edge to edge interparticle distance (b), respectively. The ECSA is calculated from CO stripping measurements and the respective measured (using ICP-MS) Pt content. TEM micrographs of the synthesized catalysts are shown at the right hand side, 30 wt% (c) 60 wt% (d) and 80 wt% (e) Pt/Ketjenblack EC-300J catalysts. Multiple layers of Pt NPs are marked by red dots.

nanoparticles on Vulcan as compared to Ketjenblack – despite the fact that Vulcan has a lower BET surface area than Ketjenblack. The carbon support dependent nanoparticle dispersion has been reported previously and can be explained by the physical and chemical properties of the used carbon blacks, *i.e.* pore structure and number of surface oxide groups, respectively.[28,29] As known from literature, Ketjenblack EC-300J with its extensive pore structure possesses a significantly higher fraction of micro- (<2 nm) and mesopores (2–20 nm) in the carbon aggregates as compared to Vulcan XC72R.[30] One could assume that Pt NPs with a size less than 2 nm can partly penetrate into these pores, which can lower the assessable electrocatalytic surface area. Furthermore, as demonstrated in our previous work, Vulcan has a larger number of oxygen groups and surface defects.[31] It has been long recognized that these adsorption sites have a key importance in the Pt NP attachment and dispersion on support materials.

Another interesting observation is, as illustrated in Fig. 2b, the fact that the onset of agglomeration of Pt NPs occurs on Ketjenblack at a higher interparticle distance in comparison with Pt/Vulcan samples. We believe that this deviation is attributed to the internal pore structure. In the calculation of the interparticle distance we did not take into account the internal pore structure, but the total BET surface area of the carbon is used. Due to the pore structure it is however unlikely that the complete BET surface area is available for particle attachment. Therefore, for the Pt/Ketjenblack samples the ipd values are slightly overestimated. This overestimation can also be seen in the TEM micrographs (Fig. 2c–e). For the 30 wt% Pt/Ketjenblack sample the calculated interparticle edge to edge distance (ipd_ee) is 15.68 nm. However, the ipd_ee estimated from the TEM micrograph (Fig. 2c) is lower, roughly 5–6 nm. By contrast for the 30 wt% Pt/Vulcan sample the calculated and estimated (from TEM) ipd_ee fits well, *i.e.* is 3.96 nm and about 3–4 nm. However, it should be pointed out that TEM is not ideally suitable to determine the ipd_ee value as a three dimensional structure is displayed in two dimensions. Here it only serves as a rough check. The TEM micrographs further indicate that the Pt NPs have an average size of 2 nm (radius of 1 nm) and that the distribution on the HSA carbon support is uniform. In line with the ECSA it is seen that average particle size does not increase with increasing loading up to very high loadings. NP agglomeration can only be observed at nominal Pt loadings above 70 wt% when Pt NPs start to form multilayer structures (indicated by red circles). These observations indicate that our catalyst samples are well suited to study the impact of particle proximity on HSA carbons.

In order to confirm the particle size distribution small angle X-ray scattering measurements were performed. The resulting Pt NP size analysis of the catalysts with varying loading is shown

in Fig. 3. In agreement with the ECSA values and TEM micrographs, the analysis of the lower nominal Pt loading reveals well dispersed Pt NPs with an average diameter of 2 nm. For the 30 wt% samples the average particle diameter for Pt/Ketjenblack is 2.2 ± 1.2 nm (FWHM as error) and for Pt/Vulcan is 1.72 ± 1.18 nm. Only at extremely high metal loadings, *i.e.* above 70 wt% Pt loading, agglomeration of the Pt NPs occurs.

In order to compare the measured ECSA values with the SAXS data, from each particle size distribution curve, we calculated a volume normalized metal surface area by using eqn (5). Thereby it is assumed that the Pt NPs are spheres and the number of NPs can be calculated from the Pt wt% determined by ICP-MS measurements. Furthermore, it should be noted that the surface areas obtained by the two methods, *i.e.* SAXS and CO stripping cannot be directly compared. The total metal surface area obtained from the X-ray scattering data does not take into account that part of the surface of the Pt nanoparticles is shielded by the carbon support. This fraction of the NP surface is electrochemically not accessible for CO molecules or other reactions. If one assumes a fraction of 30% of the surface of the individual NPs to be shielded by the carbon support, SAXS and CO stripping data lead to similar metal surface areas (see Table 1). For example, for the samples with 30 wt% nominal Pt loading, the metal surface area determined by SAXS is 88.3 and 92.2 $m^2\ g^{-1}$ for Ketjenblack and Vulcan, respectively, whereas the CO stripping measurements lead to 84.8 and 104.3 $m^2\ g^{-1}$. Note that for calculating the metal surface area the real Pt loading, as determined by ICP-MS was used and that the covered surface fraction of 30% is only an estimate based on the fact that at this value a good accordance between particle size and metal surface area is found.[5]

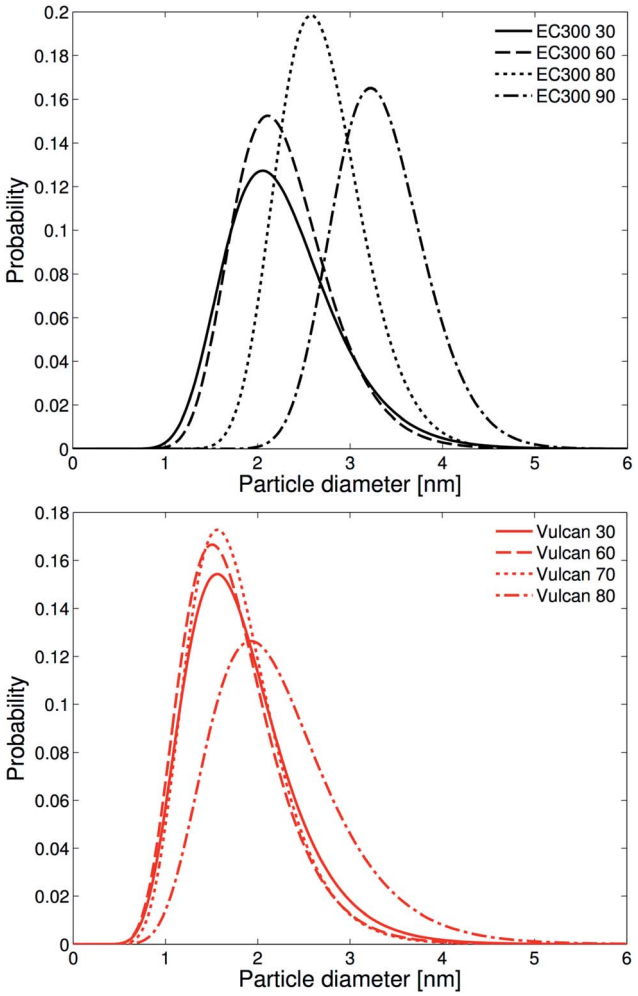

Fig. 3 Pt NP distribution curves of Pt/Ketjenblack and Pt/Vulcan samples obtained by SAXS.

3.2 Catalytic performance

The electrocatalytic performance of the Pt/C catalysts was determined using the rotating disk electrode (RDE) thin film methodology. A series of polarization curves is found in the supporting information. The electrocatalytic turnover rate, *i.e.* the surface specific activity (I_s) of the oxygen reduction reaction (ORR) was measured at 0.9 V_{RHE}. From I_s and the ECSA, determined by CO stripping, the mass specific activity (I_m) was calculated.

The surface specific activity of the ORR for a series of catalysts with various interparticle distances and carbon supports is summarized in Fig. 4. As can be seen, there is a strong correlation between the surface specific activity and the calculated average distance between nanoparticles. By lowering the interparticle distance between neighboring particles a steep increase in specific activity can be observed. The fact that the I_s *vs.* interparticle distance data are shifted to a higher interparticle distance on Ketjenblack as compared to Vulcan may indicate that there is a different relationship between activity and interparticle distance or even an electrocatalytic role of the carbon support in the ORR. However, we believe that this discrepancy is simply related to the previously mentioned pore structure properties of the Ketjenblack support and the consequently overestimated interparticle distance.

The oxygen reduction activities are also expressed in terms of A mg^{-1}_{Pt} ($I_{m(0.9\ V)}$ mass activity, see Fig. 5) in order to account for the economic potential of the catalysts. From Fig. 5 it can be seen that the mass specific ORR activity of the Pt/Vulcan samples continuously increases as a function of the Pt nominal loading (wt%). For the Pt/Ketjenblack samples a maximum in mass specific activity is achieved at around 80 wt%. This maximum is a result of the combined effect of increasing I_s and decreasing ECSA. By increasing the Pt loading to extremely high loadings, the Pt NPs form multiple layers or remain unsupported. Therefore a significant drop in the ECSA is observed over-compensating the increase in surface specific activity. Furthermore, it is observed that as a consequence of the higher ECSA of the Pt/Vulcan samples in comparison to the Pt/Ketjenblack counterparts, their mass activities are significantly higher. For Pt/Vulcan a maximum mass specific activity higher than 750 A g^{-1}_{Pt} is achieved as compared to *ca.* 610 A g^{-1}_{Pt} for Pt/Ketjenblack.

The activity data obtained here for Pt NPs supported on high surface area carbons exhibit the same trends as observed in our previous study on Pt cluster model catalysts, *i.e.* a particle proximity effect can be observed.[16] In the previous study we presented

Table 1 Comparison of the ECSA obtained by CO stripping and the metal surface area determined by SAXS for Pt/Ketjenblack and Pt/Vulcan samples

Pt/Ketjenblack EC-300J	NP radius[a] (nm)	FWHM (nm)	ECSA[b] ($m^2\ g^{-1}$)	ECSA[c] ($m^2\ g^{-1}$)
30 wt%	1.10	0.66	88.3	84.8
60 wt%	1.11	0.61	83.1	78.6
80 wt%	1.33	0.69	73.7	80.8
90 wt%	1.65	0.56	55.6	45.5
Pt/Vulcan XC72R	**NP radius[a] (nm)**	**FWHM (nm)**	**ECSA[b] ($m^2\ g^{-1}$)**	**ECSA[c] ($m^2\ g^{-1}$)**
30 wt%	0.86	0.59	92.2	104.3
60 wt%	0.83	0.55	103.4	106.8
70 wt%	0.85	0.53	101.5	100.0
80 wt%	1.06	0.72	78.6	78.9

[a] Determined by fitting experimental SAXS curves *via* eqn (1)–(4). [b] Derived from the NP distribution curves *via* eqn (5) assuming spherical particles, 30% of Pt NP surface coverage by carbon and data is corrected by real Pt wt% obtained from the ICP-MS data. [c] Determined from CO stripping and corrected by real Pt wt% obtained from the ICP-MS data.

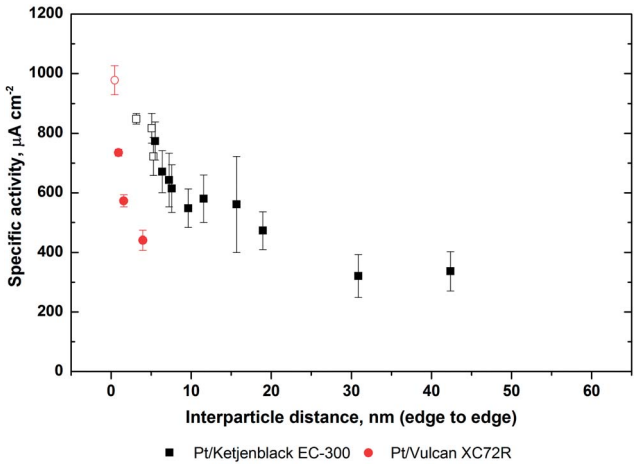

Fig. 4 Surface specific activities (I_s) of the model catalysts for ORR as a function of calculated interparticle distance (edge to edge) measured in oxygen saturated 0.1 M $HClO_4$ at 0.9 V_{RHE} and at 20 °C. The open circles and squares represent agglomerated catalyst samples. Under the same conditions I_s of polycrystalline Pt is 2 mA cm^{-2}_{Pt}.

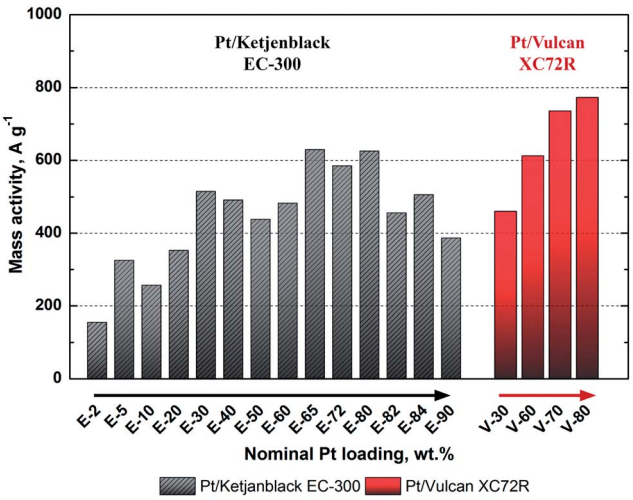

Fig. 5 Mass specific activities (I_m) of the model catalysts for the ORR as a function of the nominal catalyst loading. The mass activities were calculated from the respective specific activity and surface area.

a simple theoretical model for the particle proximity effect. Computational modeling indicated that the potential drop in the electrochemical double layer (EDL) changes if metal NPs are placed in close proximity to each other. The model of the particle proximity effect thus indicated that the EDL of the nanoclusters is a key factor to influence the coverage of an electrode with oxygenated species. According to the model the observed trend for the ORR activity of the Pt NPs is due to an overlap in the EDL between the NPs, *i.e.* the smaller the separating distance between the NPs, the larger the EDL overlap affecting the potential drop in the compact layer. The proposed model is visualized by the scheme in Fig. 6. For large interparticle distance (a) there is no overlap in the EDL, but as the interparticle distance decreases the EDL overlap increases (b and c).

We proposed that such a potential drop should lead to reduced oxide coverage at a given electrode potential. Therefore we studied the Pt oxide reduction on the Pt/C samples using cyclic voltammetry. In Fig. 7 the Pt oxide reduction peak position of the Pt/Ketjenblack samples is plotted as a function of the interparticle distance. As a reference the peak potential of polycrystalline Pt is shown as well. The peak potential varies between 0.8 and 0.75 V_{RHE} with polycrystalline Pt having the highest peak potential and the 10 wt% Pt/C sample the lowest. That is the peak potential increases as the interparticle distance is decreasing. Kumar *et al.* have previously reported similar behavior on Pt particle arrays supported on indium-tin oxide coated glass *i.e.* the peak potential of the O_2 reduction shifted to more positive values as the interparticle spacing decreased while the particle size was kept identical.[32] In their study, this potential shift was explained by the change of the extent of O_2 diffusion field overlap. In the literature, this peak potential of Pt oxide reduction is often correlated with the catalytic activity for the ORR.[33] It is assumed that OH-species are a reaction

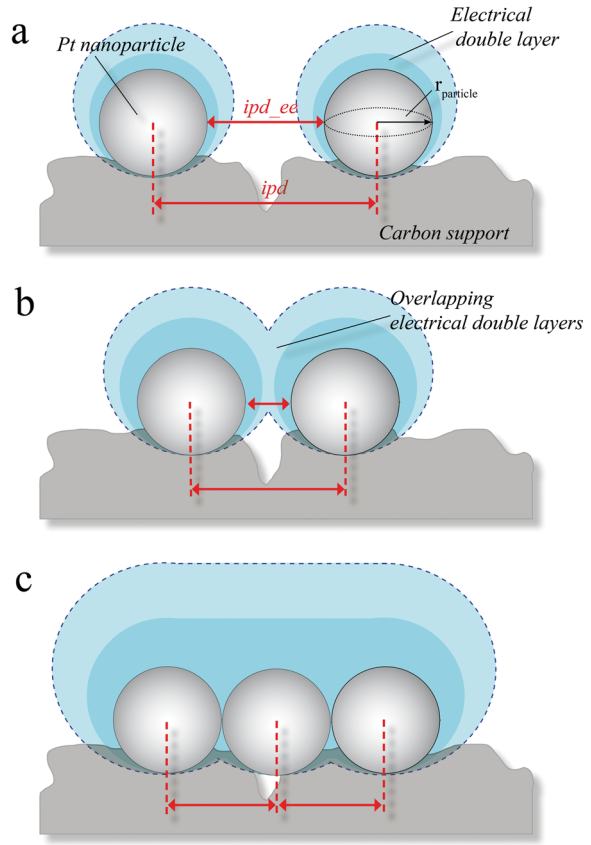

Fig. 6 Illustration of the electrical double layer (EDL) for various separation distances of the Pt NPs. For illustration purpose the EDL of the carbon substrate is not in the scheme.

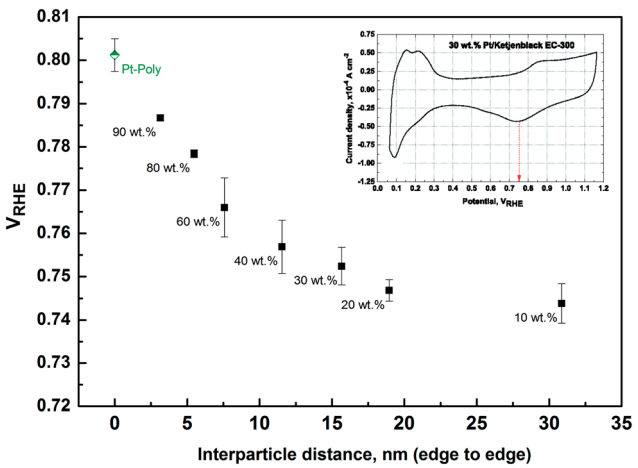

Fig. 7 Pt oxide reduction peak potentials for Pt/Ketjenblack samples with various Pt loading as a function of the calculated interparticle distance (edge to edge). The inset shows the determination of the peak potential using cyclic voltammetry recorded in 0.1 M $HClO_4$ with a sweep rate of 50 mV s^{-1} at room temperature.

intermediate as well as a blocking species depending on the adsorption strength. A shift in the Pt oxide reduction peak potential toward higher potentials reflects a less oxophilic surface, *i.e.* a lower adsorption strength of the OH-species. Indeed our results show that the increased surface specific activity of the Pt/C with increasing loading is correlated to an increased Pt oxide reduction peak potential.

4. Conclusions

In the presented study we demonstrate that the particle proximity effect first shown for Pt nanocluster model catalysts also exists for industrial PEMFC catalysts, *i.e.* Pt NPs supported on high surface area carbons. Thus in order to maximize the activity of PEMFC catalysts, one needs to increase the metal loading as much as possible (shortest interparticle distance), while at the same time avoiding NP agglomeration in order to maintain a high surface area.

Even though the observed increase in activity is less pronounced as for the extremely well defined model catalysts, a significant increase in activity can be observed for highly loaded catalysts samples. Both surface area and mass specific activities increase roughly by a factor of two when going from low to high Pt loadings. At the same time comparing the maximum achieved surface area specific activity of below 1 mA cm^{-1}_{Pt} to the value of polycrystalline Pt of 2 mA cm^{-1}_{Pt}, the results indicate that theoretically a further improvement by the factor of two in surface area specific activity might be possible for pure Pt catalysts by optimizing the electrochemical double layer. One of the next steps in our studies will be to demonstrate that the potential of such highly loaded catalysts can also be utilized in membrane electrode assemblies. Due to the high ratio of Pt to carbon surface area, we expect that for this the electrode structure, *i.e.* the blending of the different ingredients such as Nafion ionomer needs to be optimized for this kind of catalysts.

Acknowledgements

This work was supported by the Danish DFF through grant no. 10-081337 and the European Cost Action MP0903 Nanoalloys. We thank Andrea Mingers of the group of Dr Karl J. J. Mayrhofer at the MPIE for the ICP-MS analysis.

References

1 K. Kinoshita, *J. Electrochem. Soc.*, 1990, **137**, 845–848.
2 J.-H. Wee, *Renewable Sustainable Energy Rev.*, 2007, **11**, 1720–1738.
3 Y. Wang, K. S. Chen, J. Mishler, S. C. Cho and X. C. Adroher, *Appl. Energy*, 2011, **88**, 981–1007.
4 H. A. Gasteiger, S. S. Kocha, B. Sompalli and F. T. Wagner, *Appl. Catal., B*, 2005, **56**, 9–35.
5 M. Nesselberger, S. Ashton, J. C. Meier, I. Katsounaros, K. J. J. Mayrhofer and M. Arenz, *J. Am. Chem. Soc.*, 2011, **133**, 17428–17433.
6 F. J. Perez-Alonso, D. N. McCarthy, A. Nierhoff, P. Hernandez-Fernandez, C. Strebel, I. E. L. Stephens, J. H. Nielsen and I. Chorkendorff, *Angew. Chem., Int. Ed.*, 2012, **51**, 4641–4643.

7 K. J. J. Mayrhofer, B. B. Blizanac, M. Arenz, V. R. Stamenkovic, P. N. Ross and N. M. Markovic, *J. Phys. Chem. B*, 2005, **109**, 14433–14440.
8 M. Watanabe, S. Saegusa and P. Stonehart, *Chem. Lett.*, 1988, **17**, 1487–1490.
9 M. Watanabe, H. Sei and P. Stonehart, *J. Electroanal. Chem.*, 1989, **261**, 375–387.
10 H. Yano, T. Akiyama, M. Watanabe and H. Uchida, *J. Electroanal. Chem.*, 2013, **688**, 137–142.
11 P. Stonehart, *J. Appl. Electrochem.*, 1992, **22**, 995–1001.
12 H. Yano, T. Akiyama, P. Bele, H. Uchida and M. Watanabe, *Phys. Chem. Chem. Phys.*, 2010, **12**, 3806–3814.
13 H. Yano, T. Akiyama, H. Uchida and M. Watanabe, *Energy Environ. Sci.*, 2010, **3**, 1511–1514.
14 K. Hartl, M. Nesselberger, K. J. J. Mayrhofer, S. Kunz, F. F. Schweinberger, G. Kwon, M. Hanzlik, U. Heiz and M. Arenz, *Electrochim. Acta*, 2010, **56**, 810–816.
15 S. Kunz, K. Hartl, M. Nesselberger, F. F. Schweinberger, G. Kwon, M. Hanzlik, K. J. J. Mayrhofer, U. Heiz and M. Arenz, *Phys. Chem. Chem. Phys.*, 2010, **12**, 10288–10291.
16 M. Nesselberger, M. Roefzaad, R. Faycal Hamou, P. Ulrich Biedermann, F. F. Schweinberger, S. Kunz, K. Schloegl, G. K. H. Wiberg, S. Ashton, U. Heiz, K. J. J. Mayrhofer and M. Arenz, *Nat. Mater.*, 2013, **12**, 919–924.
17 J. Speder, L. Altmann, M. Roefzaad, M. Baumer, J. J. K. Kirkensgaard, K. Mortensen and M. Arenz, *Phys. Chem. Chem. Phys.*, 2013, **15**, 3602–3608.
18 Y. Wang, J. W. Ren, K. Deng, L. L. Gui and Y. Q. Tang, *Chem. Mater.*, 2000, **12**, 1622–1627.
19 T. J. Schmidt, H. A. Gasteiger, G. D. Stäb, P. M. Urban, D. M. Kolb and R. J. Behm, *J. Electrochem. Soc.*, 1998, **145**, 2354–2358.
20 E. Higuchi, H. Uchida and M. Watanabe, *J. Electroanal. Chem.*, 2005, **583**, 69–76.
21 K. Ke, K. Hiroshima, Y. Kamitaka, T. Hatanaka and Y. Morimoto, *Electrochim. Acta*, 2012, **72**, 120–128.
22 K. J. J. Mayrhofer, D. Strmcnik, B. B. Blizanac, V. Stamenkovic, M. Arenz and N. M. Markovic, *Electrochim. Acta*, 2008, **53**, 3181–3188.
23 K. J. J. Mayrhofer, S. J. Ashton, J. Kreuzer and M. Arenz, *Int. J. Electrochem. Sci.*, 2009, **4**, 1–8.
24 H. A. Gasteiger, N. Markovic, P. N. Ross and E. J. Cairns, *J. Phys. Chem.*, 1994, **98**, 617–625.
25 K. Hartl, K. J. J. Mayrhofer, M. Lopez, D. Goia and M. Arenz, *Electrochem. Commun.*, 2010, **12**, 1487–1489.
26 D. A. Stevens, S. Zhang, Z. Chen and J. R. Dahn, *Carbon*, 2003, **41**, 2769–2777.
27 T. Zemb and P. Lindner, *Neutrons, X-rays and light: scattering methods applied to soft condensed matter*, Elsevier, 2002.
28 J. Speder, A. Zana, I. Spanos, J. J. K. Kirkensgaard, K. Mortensen and M. Arenz, *Electrochem. Commun.*, 2013, **34**, 153–156.
29 A. Zana, J. Speder, M. Roefzaad, L. Altmann, M. Baumer and M. Arenz, *J. Electrochem. Soc.*, 2013, **160**, F608–F615.
30 T. Soboleva, X. Zhao, K. Malek, Z. Xie, T. Navessin and S. Holdcroft, *ACS Appl. Mater. Interfaces*, 2010, **2**, 375–384.
31 A. Zana, J. Speder, N. E. A. Reeler, T. Vosch and M. Arenz, *Electrochim. Acta*, 2013, **114**, 455–461.
32 S. Kumar and S. Zou, *Electrochem. Commun.*, 2006, **8**, 1151–1157.
33 P. J. Ferreira, G. J. laO', Y. Shao-Horn, D. Morgan, R. Makharia, S. Kocha and H. A. Gasteiger, *J. Electrochem. Soc.*, 2005, **152**, A2256–A2271.

